LAWRENCE
LIVERMORE
NATIONAL
LABORATORY

LLNL-CONF-675617

On Mesoscale Methods to Enhance Full-Stress Continuum Modeling of Porous Compaction

M. A. Homel, E. B. Herbold

July 30, 2015

American Physical Society Shock Compression of Condensed Matter
Tampa, FL, United States
June 14, 2015 through June 19, 2015

Disclaimer

On Mesoscale Methods to Enhance Full-Stress Continuum Modeling of Porous Compaction

Michael A. Homel[1,a)] and Eric B. Herbold[1,b)]

[1]*Lawrence Livermore National Laboratory, 7000 East Ave. Livermore, CA 94550.*

[a)]homel1@llnl.gov
[b)]herbold1@llnl.gov

Abstract. The dynamic compaction of initially porous material is typically treated in continuum dynamics simulations via adjustments to the scalar equation of state (EOS) of the bulk, porous material relative to that of the solid. However, the behavior during compaction is governed by inelastic processes, as the solid material deforms, largely by shearing, to fill the voids. The resulting response depends on the strain path, e.g. isotropic versus uniaxial loading. Adjustments to the EOS are therefore fundamentally unsuited to describing porous compaction, and it is desirable to consider porous effects through the stress and strain tensors. We have performed mesoscale simulations, resolving the microstructure explicitly, to guide the construction of continuum models. These simulations allow us to study the interplay between strength and EOS in the solid, the extent of dissipative flow versus non-dissipative displacement, and the evolution of porosity and micro-morphological features.

INTRODUCTION

A common approach to continuum modeling of porous compaction is to decouple the isotropic and deviatoric responses, using separate models to evaluate the equation of state and the shear strength. This approach can give accurate results, even when shear work significantly affects the material pressure, but only when the experimental data used to parameterize the continuum model is for the same mode of deformation as that for which the model will be applied. The vast majority of high-rate material characterization is obtained through experiments that produce a 1-D uniaxial strain shock wave, so that the Hugoniot equations can be applied to infer the material state from measurements of the particle and shock velocities. In penetration events into brittle solids or soils, significant deformation occurs with relatively high shear and moderate pressure, the pressure-volume response may be quite different from that observed in uniaxial strain compaction.

To capture the effect of shear work for generalized loading it is necessary to construct a thermo-mechanical model, in which the yield surface is a function of the stress (σ), the internal energy (u) (or temperature), and possibly other history-dependent state variables (*e.g.,* damage or porosity). When the strength depends on pressure, it is necessary to employ a full-stress model to compute the plastic flow direction. For porous materials, the volumetric plastic strain significantly affects both the strength and elastic properties, so it is particularly important to account for the coupling effect.

Many full-stress thermo-mechanical constitutive models exist (*cf.,* Fuller *et al.* [1] or Vorobiev [2] for geomaterials, Bar-on *et al.* [3] for ceramics, or Quidwai *et al.* [4] for porous shape memory alloys). Such models have the potential to be highly predictive over a broad range of loading regimes, but have many input parameters requiring significant experimental paramterization. In many cases, analysts will use unrealistically simple models when the data needed to properly use a more sophisticated model is impractical to obtain. Analysis of mesoscale simulations has the potential provide virtual data that can be used for model parameterization, reducing the need for experiments and in many cases providing data for loading modes that are difficult to characterize experimentally. This is particularly true for granular and porous materials where much of the bulk material response is governed by evolution of micromorphology, and where the response of the solid phase is relatively well characterized.

High-rate materials characterization typically involves experiments that have been designed to achieve a steady 1-D shock, so that the Rankine–Hugoniot conditions can be applied to calculate the pressure and density from the

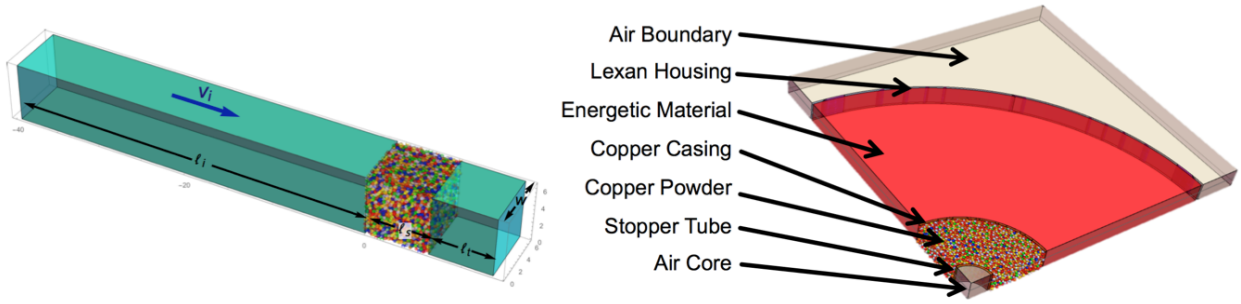

FIGURE 1. Simulation geometry: (a) uniaxial strain powder compaction (b) axisymmetric radial compaction.

observed particle and shock velocities [5]. In recent years, several researchers have demonstrated that mesoscale models can reproduce the Hugoniot data for shock experiments on granular and porous materials [6, 7].

While matching experimental results is a necessary validation, the great value in mesoscale simulation is that a wealth of information about the dynamic material state becomes accessible, without the limitations of traditional experimentation. Averaged values for the pressure ($\bar{p}$), density ($\bar{\rho}$), and internal energy ($\bar{u}$) can be obtained for a region of the mesocale domain, without requiring the existence of a steady-state shock. Because of this, it is possible to design experiments that probe a broad range of states in the $\rho - u - p$ space. In contrast, traditional experimental methods provide only a single point on the Hugoniot curve for a given material.

In designing mesocale simulations, it is tempting to prescribe a uniform initial velocity gradient with compatible Dirichlet boundary conditions, in order to obtain a desired loading path for the material. However, for high-rate loading of heterogenous materials, particularly those for which the density varies significantly between the constituents, this approach is flawed. In actual high-rate loading, the effect of a shock front causes micro-kinetic effects that may produce significant distortion of individual grains, and a corresponding contribution to the thermal pressure in the material. In contrast, a high rate loading with an initially uniform velocity field produces a self-similar deformation, dominated by inertial effects, with significantly less grain-scale distortion [8].

The challenge is then to define a mesoscale simulation that probes a wide range deformation states while locally deforming that material with a shock front (rather than a prescribed deformation). Furthermore, it is desirable to control of the strain rate, the initial and final compaction, and the relative amount of shear vs. volumetric loading. To this end we have explored the use of mesoscale simulation of a powder compaction using a configuration similar to the thick-walled cylinder collapse, used by Nesterenko to study shear banding formation and deformation of pre-fractured ceramics [9].

METHODS

Mesoscale simulations use GEODYN, an Eulerian hydrocode with high-order interface reconstruction and a modified Godunov scheme. This method has been demonstrated to accurately resolve shock loading and it accurately (by-construction) conserves energy [10], which is essential when extracting equation of state response from the simulation results. Previous work by Lomov, *et al.* [6] demonstrated that 3-D mesoscale analysis of porous compaction of aluminum using GEODYN could reproduce experimental results for 1-D shock loading.

We simulate compaction of a packed bed of spherical copper particles with a solid volume fraction 0.6271. The particle diameter ranges from 297.0μm to 420.0μm, with a mean of 358.5μm. The particle packing is produced with the SnowNinja discrete element method (DEM) code. The solid phase is modeled with a Mie-Gruneisen equation of state and a Steinberg-Guinan model for the dependence of strength on pressure and temperature. The initial solid density is 8.93mg/mm^3.

For this analysis we consider two loading scenarios as shown in Fig. 1. The first is a uniaxial strain with a rectangular incident bar with length l_i = 40mm and initial velocity v_i = 0.375mm/μs impacts a powder bed of length l_s = 7mm followed by a transmission bar of length l_t = 7mm. The cross section is square with width w_i = 7mm.

The second geometry is an axisymmetric radial compaction; the geometry is a $1/4$ annular bed of 8305 packed spheres, with an inner diameter, outer diameter and height of 3.18mm, 11.1mm, and 3.585mm, respectively. The

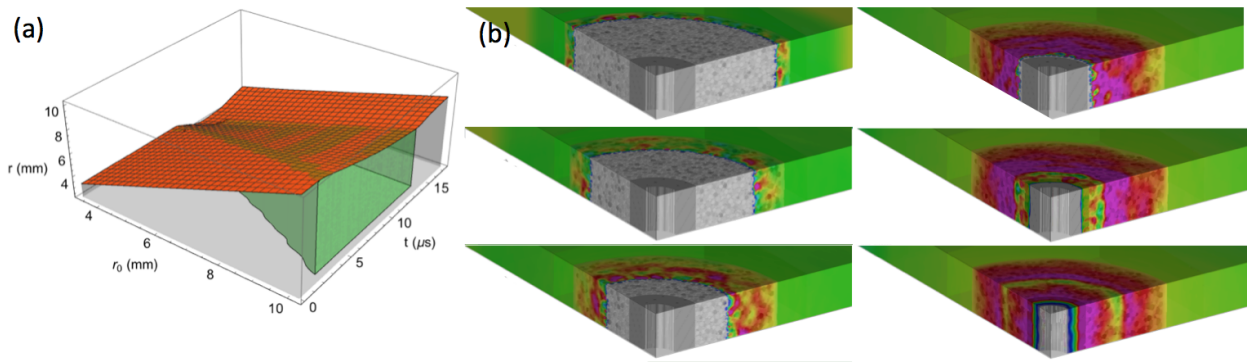

FIGURE 2. (a) Bulk radial motion $r(r_0, t)$ for TWC compaction, with the initial compaction highlighted in green. (b) Contours of pressure during the initial compaction.

collapse is driven by the expansion of an energetic material, which is modeled as an ideal gas with initial density $\rho_0 = 1.0\text{mg/mm}^3$, and initial energy density $u_0 = 1.5\text{J/mm}^3$. The model geometry and particle size were selected based on experimental results for porous compaction in a thick-walled cylinder geometry, in an effort to avoid shear band formation, so the particle bad can be treated as a continuum.

To extract the history of a Lagrangian volume from the Eulerian simulation results, we define a mapping $r(r_0, t)$ to characterize the homogenized bulk radial motion. A set of Lagrangian markers are defined, which are initially at the centers of 200 randomly selected particles. The location of these markers is updated explicitly throughout the simulation. The average radial motion is then fit to a time-history of the markers. This implicitly defines the bulk material motion as that of the particle ensemble, essentially neglecting the effect of any air displacement relative to the particles during consolidation.

In constructing the radial motion from the marker data, it is desirable to obtain a smooth function $r(r_0, t)$ that represents the bulk continuum motion so that the spatial and temporal gradients can be used to analyze the kinematics. Point-to-point variations in the marker data preclude a simple interpolation of the raw data, so we first resample the data with local averages at a uniform radial spacing, and then construct a piecewise Hermite interpolation of the resampled points. The bulk radial motion is plotted in Fig. 2a.

For some spatially varying field $f(r, \theta, z, t)$ (*e.g.,* the pressure, density, internal energy etc.), the nominal continuum value $\bar{f}(r, t)$ is computed by a volume average over a quarter annulus subregion of the powder volume. The averages are computed using VisIt, which accounts for the varying mesh density with adaptive mesh refinement. In defining these average values over some portion of the domain, the size of the averaging region relative to that of the shock front can affect the computed result. It is desirable to have the domain be as small as possible, to avoid significant variations in the nominal pressure across the region, while also having the domain be large enough that point-to-point variations do not introduce significant noise. For our simulations, a smooth representation of the density and pressure fields could be obtained when the slice thickness was at least $1/2$ particle diameter. Increasing the height of the simulation domain would allow for improved spatial resolution by reducing noise due to local variations.

We rotate the local stress based on its current position and compute a volume average of the radial, circumfrential and axial stresses over the annular regions. During the initial compaction stage, the shear stress increases monotonically and the plastic deformation front is coincident with the pressure wavefront. This suggests that the stress is on the yield surface throughout the initial compaction phase, so the shear stress can be interpreted as a shear strength τ_Y, which can be expressed as a function of $\bar{\rho}$ and $\bar{u}$. For a radial motion, the principal directions are r, θ, and z, so the deformation in the cylindrical reference frame is a pure stretch with $\mathbf{F} = \text{DIAG}(F_{rr}, F_{\theta\theta}, F_{zz})$. From the radial motion we have

$$F_{rr}(r_0, t) = \frac{\partial r(r_0, t)}{\partial r_0} \tag{1}$$

With symmetry enforced on the $+z$ and $-z$ faces, $F_{zz} = 1$, so with $\bar{\rho} J = \bar{\rho_0}$, and $J = \det \mathbf{F}$,

$$F_{\theta\theta}(r_0, t) = \frac{\rho_0}{\rho(r_0, t)} \frac{1}{F_{rr}(r_0, t)}. \tag{2}$$

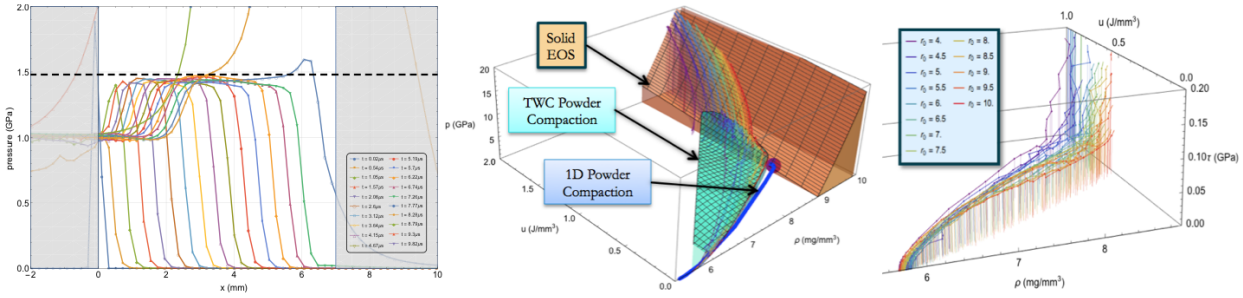

FIGURE 3. Pressure in the 1d bar from averages of slices of the domain normal to the wave propagation. The dashed line shows the pressure computed from the particle and shock velocities. (top) Pressure vs. density and internal energy for the thick-walled cylinder powder compaction and a 1-D uniaxial strain powder compaction, shown relative to the solid EOS. (center) Dependence of shear strength on density and internal energy during the initial compaction phase of the TWC. (bottom)

The time dependence of $\mathbf{F}$ also lets us compute the strain rates applied to the bulk simulation. For the TWC simulation, using a Lagrange strain measure, the peak strain rate depends on radius and ranges from 1×10^5 to $1 \times 10^6 \mathrm{s}^{-1}$, however this range is approximate since calculation of the strain rate is sensitive to noise in the fit to the radial motion. By varying the intensity of the explosive, it is possible to achieve a broad range of strain rates, and thus to characterize the effect of strain rate on the $\bar{\rho} - \bar{u} - \bar{p}$ behavior.

The material is unloaded upon the arrival of the release wave from the the stopper tube. Using the rates of the deformation gradient and the averaged stresses, we obtain a value for the elastic tangent properties at this state. Since the pressure and density vary radially at the point of unloading, this provides elastic properties for a range of states. The unloading response can be seen more clearly by using a thick, low-impedance stopper tube. However, for this analysis, the radial motion field was too noisy to obtain meaningful results for the elastic properties.

To provide a metric for estimating the error in the bulk continuum motion, we can compare the spatially averaged density field with that computed from the kinematics, $\rho(r_0, t) = \frac{\bar{\rho}_0 r_0}{r(r_0,t)} / \left(\frac{\partial r}{\partial r_0}\right)_t$. For the TWC simulations, the results compare well during the initial compaction phase, but there is significant error at the inner radius after unloading and during the subsequent collapse and reshock.

A second error metric, which is more sensitive to the temporal gradient of the radial motion, is the comparison of the rate of internal energy computed from the spatial averages compared to the computed stress work. Neglecting the kinetic energy effect, and in the absence of a source term, the change in internal energy for adiabatic deformation is the stress power, $\dot{u} = \mathbf{P} : \dot{\mathbf{V}} = \frac{1}{\rho_0}\mathbf{t} : \dot{\mathbf{F}}$, where $\mathbf{t}$ is the first Piola-Kirchoff stress $\mathbf{t} = J\sigma \cdot \mathbf{F}^{-T}$. Both methods generally agree well, indicating there is consistency in the calculation of stress, density, and motion, and internal energy, but there is a clear discrepancy at the shock front.

Several methods are available to reduce the analysis error, (i) increase the the height of the computational domain to smooth point-to-point fluctuations and allow a decreased radial slice width, (ii) increase the mesh resolution to reduce the fraction of mixed cells, (iii) increase the number of Lagrangian markers to better capture the radial motion, (iv) improve the construction of the radial motion field from Lagrangian markers to eliminate noise while preserving key features. The density and energy rate metrics provide a means to assess convergence, which is important since each of these approaches comes with an increase in computational expense.

RESULTS

The 1-D porous compaction simulation is analyzed to compare the results from spatial averages over slices normal to the wave propagation direction to those obtained using a conventional impedance matching analysis. Interpreting the Eulerian field velocity as the particle velocity $u_p(x)$, we then solve for the shock velocity u_s that minimized the standard deviation in the aligned shock fronts $u_p(x - u_s t)$. Computing the initial density $\bar{\rho}_0$ from volume averages over the initial domain, we then compute the Hugoniot pressure as $p^\star = \bar{\rho}_0 u_s u_p$. Figure 3a shows the pressure from spatial averages at various times in the simulation, which agrees reasonably well with the Hugoniot pressure. The discrepancy is likely due to boundary effects.

The ratio of the specific volume V to the initial specific volume V_0 is computed from the velocities $V/V_0 =$

$1 - u_p/u_s$, which is used to compute the Hugoniot density, $\rho^\star = \bar{\rho_0} V_0/V$. With these values we then compute the volumetric internal energy $u^\star = \frac{1}{2}\rho^\star p^\star (V_0 - V)$. The spatially averaged data for $\bar{p}$, $\bar{\rho}$, and $\bar{u}$ from the 1-D compaction data trace a curve in state space as shown in Fig. 3b. The Hugoniot point $[\rho^\star, u^\star, p^\star]$ is plotted along with this data, and falls on the line. This provides verification for the analysis method and confirms that the spatial averaging of the Eulerian fields gives a result consistent with a traditional shock analysis.

Figure 2b shows contours of pressure during the initial porous compaction of the TWC collapse. The initial porous compaction shows a sharp shock front, but there are significant point-to-point variations in the stress field. A release wave initiates at the outer surface of the low-impedance stopper tube unloading the material. Once this wave hits the outer surface of the particle bed, the reflection recompresses the material. This occurs as the core collapse, along with high shear flow near the inner radius of the powder bed. Once the core collapses completely, a high pressure wave propagates outward, followed by a radial expansion. The stresses in this final stage are much higher than during the porous compaction, which points to the need for dynamic, *in-situ* experimental validation of the initial dynamic response, since a post-mortem analysis could be significantly hindered by this post-compaction deformation.

Figure 3b shows the pressure for each radial slice of the TWC domain versus density and internal energy, along with the results from the 1-D compaction simulation. The equation of state of the solid material is plotted for reference. The results show a very significant effect of shear deformation on the overall response, with the pressure at a given density increasing (by a factor of ≈ 2) towards the inner radius of the particle bed.

Shear strength during porous compaction is plotted in Fig. 3c, showing that for a given density the shear strength increases with internal energy, most significantly as the density approaches the solid density. The solid phase softens as the internal energy is increased, but the solid also expands so that for a given bulk density, the material with the higher internal energy as a lower porosity. Thus, the results indicate that for this material the geometric effect due to thermal expansion dominates the thermal softening effect in the solid material.

DISCUSSION AND CONCLUSION

The results show that the effect of shear work is significant on the $p - \rho$ response, and should be taken into account when developing continuum constitutive models for porous materials. The use of 1-D shock loading experiments to parameterize the equation of state response for granular (or more generally, for highly porous materials) is therefore only sufficient when the model is to be used for a region of the computational domain that will be subjected to a 1-D uniaxial strain shock. While this mode of deformation may dominate for material subject to blast loading far from the energetic source, it would not adequately approximate the loading state in a penetration event.

However, simply showing that the shear work produces a non-negligible thermal pressure is not sufficient to show that a full-stress model is needed. An iterative decoupled model would still produce increase plastic work and associated thermal pressure in shear loading relative to hydrostatic compression. It will be necessary to reproduce the mesoscale result with a continuum simulation to understand how details of the constitutive model's numerical solution affects the macroscale response. In this way the mesoscale results can guide the development of more predictive continuum models.

This approach can be extended to investigate the porous compaction response of a variety of materials with varying mechanical properties and morphologies. A key limitation will be avoiding radial shear localization, which would break axisymmetry and would invalidate the continuum analysis. Experimental work[9] has shown that shear banding will occur for fine particles, but it is not clear from available experimental results whether this initiates during the porous compaction stage, or in the subsequent shear-flow as the stopper tube collapses.

Extending the method to brittle materials will require a treatment of fracture, comminution, and frictional dissipation, which can be difficult to capture with an Eulerian approach. Lagrangian codes can more accurately described contact and fracture, but do not tolerate extreme deformation. A variety of ALE, particle, and meshless methods exist, but each has its limitations with regards to multiple phases, contact, fracture, energy conservation, and robustness. Moving forward it will be necessary to conduct *in-situ* validation of the TWC dynamic response during compaction to ensure that the numerical method is adequately describing the physical system.

Mesoscale simulation of axisymmetric radial compaction of a powder bed has been shown to produce data for the equation of state and strength over a wider range of states than a corresponding 1-D compaction simulation. This reduces the number of simulations needed to parameterize a constitutive model, which makes it practical to employ sophisticated numerical methods and constituent constitutive models with a sufficient resolution to resolve the fine scale deformation over domains of thousands of particles.

ACKNOWLEDGMENTS

This work was performed under the auspices of the U.S. Department of Energy by Lawrence Livermore National Laboratory under contract DE-AC52-07NA27344. Lawrence Livermore National Security, LLC. LLNL-CONF-675617.

REFERENCES

[1] T. Fuller, R. M. Brannon, O. E. Strack, and J. Bishop, "Initial inclusion of thermodynamic considerations in kayenta," Sandia report, SAND2010-4687 (2010).

[2] O. Vorobiev, "Generic strength model for dry jointed rock masses," International Journal of Plasticity **24**, 2221–2247 (2008).

[3] E. Bar-On, M. Rubin, and D. Yankelevsky, "Thermomechanical constitutive equations for the dynamic response of ceramics," International journal of solids and structures **40**, 4519–4548 (2003).

[4] M. A. Qidwai, P. B. Entchev, D. C. Lagoudas, and V. G. DeGiorgi, "Modeling of the thermomechanical behavior of porous shape memory alloys," International Journal of Solids and Structures **38**, 8653–8671 (2001).

[5] K. T. Ramesh, in *Springer handbook of experimental solid mechanics* (Springer, 2008), pp. 929–960.

[6] I. Lomov, D. Fujino, T. Antoun, and B. Liu, "Mesoscale simulations of powder compaction," in *Aip Conference Proceedings*, Vol. 11, edited by M. Elert, M. D. Furnish, W. W. Anderson, W. G. Proud, and W. T. Butler (2009) p. 1327.

[7] J. P. Borg and T. J. Vogler, "Mesoscale calculations of the dynamic behavior of a granular ceramic," International Journal of Solids and Structures **45**, 1676–1696 (2008).

[8] M. A. Homel, "Elastoplastic constitutive modeling of fluid-saturated porous materials with new methods for numerical solution and mesoscale validation," Ph.D. thesis, University of Utah 2015.

[9] V. Nesterenko, *Dynamics of heterogeneous materials* (Springer Science & Business Media, 2013).

[10] E. Herbold, J. Owen, D. Swift, and P. Miller, "Simulations of defense strategies for bennu: Material characterization and impulse delivery," Procedia Engineering **103**, 173–180 (2015).